Experimental characterization of a Si-Mo-Cr ductile cast iron

Technical Report

Experimental characterization of a Si–Mo–Cr ductile cast iron

Cristiana Delprete, Raffaella Sesana *

Department of Mechanical and Aerospace Engineering, Politecnico di Torino, 10129 Torino, Italy

A B S T R A C T

High temperature-resistant ductile cast irons behavior is highly interesting for the manufacture of com-ponents, such as exhaust manifolds for automotive applications. In the present paper the temperature-dependent static, high cycle and low cycle fatigue behavior of a heat-resistant Si–Mo–Cr ductile cast iron (Fe–2.4C–4.6Si–0.7Mo–1.2Cr) is investigated. Tensile and high cycle fatigue properties, in terms of elastic modulus, yield stress, elongation at break, fatigue limits, and the stress-life Basquin's curve parameters have been determined at room temperature, 160 °C, 500 °C and 800 °C, thus covering the usual temper-ature range to which actual components, obtained with this kind of material, are subjected. The alloy showed good monotonic properties at low temperature, but showed to be fragile during fatigue tests, due to the high Silicon content in the alloy. At 500 °C mechanical properties are still good, with a 40%decrease with respect to 160 °C, and ductility is increased. The last temperature level of 800 °C has caused a noticeable drop of the cast iron strength, due to softening and oxidation effects.

1. Introduction

Ductile cast irons are used for several industrial applications due to their favorable mechanical properties and low costs; their main material properties are good oxidation and thermal fatigue resistance [1–3]. The common feature of all ductile cast irons is the roughly spherical shape of the graphite nodules. These nodules act as crack-arresters and make consequently the iron to be more ductile. With a high percentage of nodules presents in the structure, the mechanical properties are determined by the ductile iron matrix [4].

If the matrix is ferritic, the graphite spheroids provide good ductility and impact resistance with a tensile and yield strength comparable to low carbon steel. The ferritic–pearlitic matrix is the most common grade, where graphite spheroids are in a matrix containing both ferrite and pearlite; properties are intermediate between ferritic and pearlitic grades, with a good machinability and low production costs. The pearlitic matrix provides an iron with high static strength, good wear resistance, moderate ductility and impact resistance. For some peculiar applications the matrix can also be martensitic, when it is produced with a quench-and-temper heat treatment and preventing pearlite formation, resulting in a very high strength and wear resistance but with lower levels of ductility and toughness. When good corrosion and oxidation resistance, good magnetic properties, and good strength and dimensional stability at high temperatures are needed, an austenitic matrix can be used. Moreover, austempered matrix is also available, characterized by strength nearly twice than pearlitic iron and a still high elongation and toughness: this combination provides a material with high wear resistance and fatigue strength.

For high-temperature applications, Si and Mo are usually added to ferritic ductile iron to improve the high-temperature mechanical properties [2,5,6]. Si addition usually causes solid solution strengthening of the ferrite matrix, stabilizing it and forming a Si-rich surface layer that inhibits oxidation. The oxidation protec-tion offered by Si increases with increasing Si content. Si levels above 4% are usually enough to prevent any significant weight gain after the formation of the initial oxide layer. In addition, increasing the Si content increases the yield and tensile strengths and reduces elongation at room temperature (RT). However, it was reported that the ductility was reduced substantially at a Si content higher than 5 weight% [2]; consequently many high-temperature applications use Si added ductile cast iron with a Si content between 4 and 5 weight%. The solid solution strengthening effect of Si persists to temperature as high as 540 °C, but above this level the tensile strength of high-Si alloys is decreased.

Mo is known as a strengthening element for ductile cast iron through the formation of carbides. Such carbide formation was reported to increase the tensile strength, thermal fatigue life, and creep resistance [2]. However, in many structural applications, Mo addition is limited to a maximum of 1 weight% in order to avoid brittleness and shrinkage defects, maximizing the resistance to thermal fatigue [4].

The problem of a unified treatment of the stress–strain-life experimental data has been described in [7]. A deep experimental activity is run on 9 ductile irons and an analysis of how standard testing results are reliable is presented. In particular strain controlled LCF fatigue testing, stress controlled HCF testing, static

* Corresponding author. Tel.: +39 011 0906907; fax: +39 011 0906999.
E-mail address: raffaella.sesana@polito.it (R. Sesana).

Nomenclature

α	thermal expansion coefficient ($°C^{-1}$)
ε_{th}	thermal strain (mm/mm)
ΔT	thermal increment (°C)
μ, s	lognormal distribution parameters of SN curves, respec-tively mean value and standard deviation (–)
C_0, C_1, C_2, D_0, D_1	coefficients related to the lognormal model of SN curves (–)
N	number of cycles (–)
σ	fatigue stress level (MPa)
R	strain or stress fatigue ratio, corresponding to maxi-mum over minimum strain or stress values (–)
σ_a	fatigue stress amplitude (MPa)
σ_m	mean fatigue stress (MPa)
$\sigma_{D0.1}$	fatigue limit in tensile–tensile fatigue tests, strain ratio $R = 0.1$ (MPa)
$\sigma_{D\text{-}1}$	fatigue limit in alternate symmetric fatigue tests (MPa)
UTS	ultimate tensile stress (MPa)
σ'_f, b	material parameters, respectively (MPa) and (–)
N_f	number of cycles to failure (–)

testing, hardness measurements and optical microscopic investiga-tions results are presented.

Microscopic investigations are applied to investigate different aspects of the cast irons mechanical behavior. In [8] a cast iron engine component, a camshaft, is investigated by means of FEM casting simulations and mechanical properties are experimentally measured by means of micro-hardness measurements. An analysis of the microstructure is obtained by means of an optical microscope in points of the camshaft, which experience different cooling histories. The focus of the paper is on the relation between microstructure and thermal transition during cooling and the effectiveness of the software to predict mechanical properties. In [9] the same microscopic investigations are applied to the determination of local complex strain state in a ductile cast iron.

In [10] the relation between thermal treatments, composition and microstructure in a white cast iron is investigated by means of optical microscopy, TEM, hardness and fracture toughness measurements.

In [11] a Round-robin experimental research results on the prediction of the fatigue limit of a spheroidal graphite cast iron are presented. In [12] an experimental activity in thermal fatigue of cast irons for automotive application is presented. In particular the relation between thermal damage and microstructure is investigated. In [13–15] mechanical properties of cast irons are described by means of static tests and micrographic and hardness measurements.

The experimental characterization described in the present paper aims to an enrichment of the lack of literature regarding the static, high cycle fatigue (HCF) and low cycle fatigue (LCF) behavior of a commercial heat resistant Si–Mo–Cr cast iron, commonly used for automotive exhaust manifolds manufacture, which requirements are mainly a good oxidation and thermal fatigue resistance. The material underwent tensile, HCF and LCF testing at many temperature levels in the range between room temperature and 800 ° C, that is the working temperature range an automotive exhaust manifold is subjected to. The results obtained from the experimental activity here presented may be used to calibrate con-stitutive and damage models used during the virtual simulations of exhaust manifolds material response under thermo-mechanical loading conditions.

2. Materials and methods

The experimental testing was conducted on the heat-resistant Si–Mo–Cr ductile cast iron, whose nominal composition is shown in Table 1. This cast iron has been provided as in-cast state in the shape of sprues from the casting process of automotive exhaust manifolds.

Before machining the specimens, all cast iron sprues have been subjected to the thermal treatment depicted in Fig. 1 in order to obtain a microstructure as similar as possible to the material of actual exhaust manifolds.

The thermal treatment consists of a single thermal cycle with a preliminary heating from room temperature up to 940 °C following a ramp of 300 °C/h, an hold time of 3 h at 940 °C, and a cooling phase defined by a ramp of 85 °C/h from 940 °C to 750 °C. Finally, at 750 ° C the furnace has been switched off and the sprues have continued their cooling at room temperature.

Static, HCF and LCF tests have been performed partially at the Mechanics Laboratories of the Politecnico di Torino - Italy, and partially at the CEROC Research Center and at the Laboratoire de Mécanique et Rhéologie (LMR) of the École d'ingénieurs Polytechnique de l'Université François Rabelais in Tours - France. The RT tests have been performed in Italy while the high temperature tests have been carried out in France along with the microstructural observations.

Monotonic and LCF characterizations at RT have been run on a servo-hydraulic testing machine INSTRON 8801, load cell Dynacell 2527 100 kN, with hydraulic wedge action grips. The resulting strain has been measured by means of an extensometer 25 mm gage length, travel [−2.50, +12.50] mm. LCF and static tests at RT have been performed on specimens as shown in Fig. 2(a), according to ASTM Standards ASTM: E 8/E 8M and ASTM: E 606. LCF and static tests at high temperature have been performed on INSTRON electro-thermomechanical testing machine INSTRON 8800 with load of 3 kN; a dedicated designed grips made by high temperature resistance AISI 310 stainless steel were used for the specimens mounting on the machine. The specimens, shown in Fig. 2(b), are smaller than those adopted for RT tests to avoid load cell overloading. HCF tests campaign has been carried out at the same temperature levels used for the static characterization, except for RT due to the high fragility of the material. It has not been possible to run RT HCF tests because the specimens failed shortly after maxi-mum load application, even for low amplitude loads. Experiments have been performed by an electromechanical resonant load-con-trolled fatigue testing machine, an Amsler Vibrophore 10 HPF 422 load cell 100 kN, determining the fatigue limit at 2×10^6 -cycles through the staircase methodology, according to UNI 3964 [16]. The cyclic testing frequency has been in the range between about 150 and 180 Hz, depending on the testing temperature. To perform HCF tests at high temperature, the vibrofore is equipped by an electric resistance oven that can be mounted around the grips and the specimen. HCF specimen geometry has been imposed

Table 1
Chemical composition of the Si–Mo–Cr ductile cast iron (weight%).

C	S	iM	Fn	S	C	iM	Nb	IM	Cg	u
2.45	4.60	0.24	0.02	0.01	1.18	0.75	0.02	0.04	0.03	

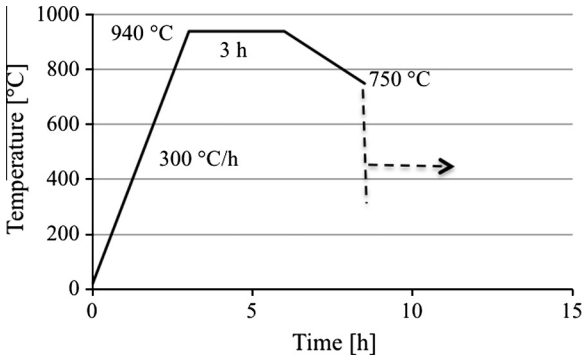

Fig. 1. Details of the thermal treatment.

by the grip system of the resonance fatigue machine, as depicted in Fig. 2(c).

The LCF strain controlled fatigue tests, along with result processing have been run according to [7] standard practice procedure. The same for HCF testing but with a higher loading frequency. The specimen fracture surfaces have been observed by a scanning electron microscope (SEM) in order to evaluate the typologies of failure.

The static behavior of the Si–Mo–Cr cast iron has been investigated at four temperature levels corresponding to RT, 160 °C, 500 °C, and 800 °C. In each condition several specimens have been tested in order to obtain at least three acceptable results. In addition, all the test pieces for high temperature tests have been held at the desired temperature for at least 20 min before starting the experiment in order to avoid thermal gradients across specimens. The crosshead speed has been set to 2 mm/min.

The Young modulus has been estimated through a linear regression interpolating the experimental data belonging to the elastic field data, excluding the ones corresponding to very low loads in which the load cell measurement accuracy is not optimum: the value of the Young modulus has been then calculated as the slope of the regression.

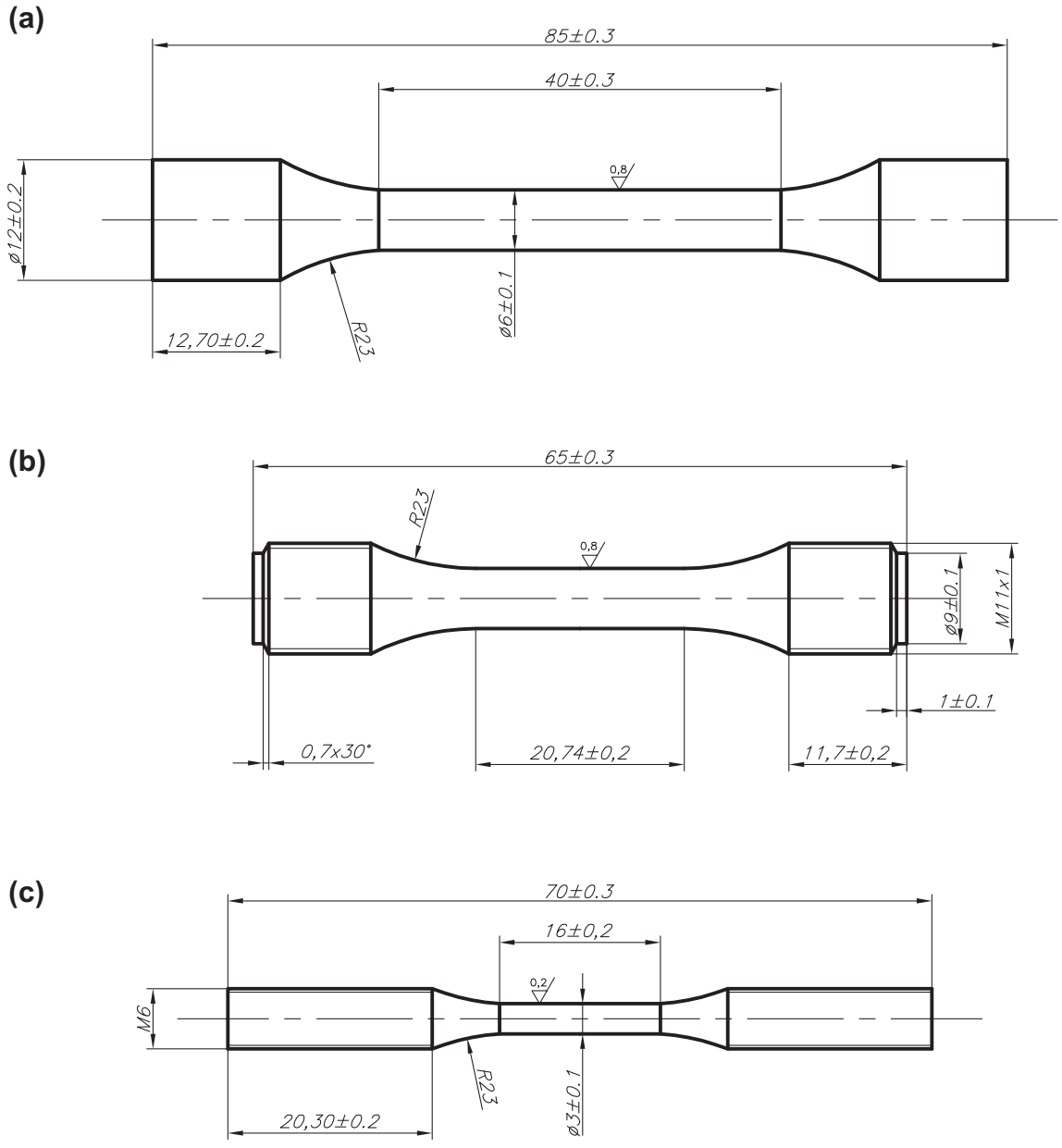

Fig. 2. Geometrical features of the specimens used in tensile and LCF tests at room temperature (a), tensile and LCF tests at high temperature (b), and HCF tests (c).

The yield stress has been estimated as the intersection between the tensile curve and a line parallel to the elastic field regression starting from 0.2% of total strain, while for the ultimate tensile strength the maximum stress achieved during the test has been considered, according to the ASTM Standards ASTM: E 8/E 8M and ASTM: E 606-98 [17,18].

The elongation at break has been measured on the test pieces after failure because the extensometer has been removed before failure, in order to avoid damage.

High temperature static tests allowed estimating the values of the thermal expansion coefficient. During the heating phase the testing machine control has been adjusted in order to ensure zero load on the specimen, resulting in a correction of the actuator position to take into account the thermal expansion of the material. The difference between the actuator position at the end of the heating phase and the initial position, divided by the initial distance between the grips, has provided the thermal strain at each temperature level. The thermal expansion coefficient has been determined as $\alpha = \varepsilon_{th}/\Delta_T$.

HCF tests have been run following the specifications of the Staircase method described in UNI 3964 Standard [16]. In order to estimate the endurance limit of the cast iron, a step equal to 10 MPa on the maximum stress, which corresponds to a step of 4.5 MPa on the stress amplitude, has been chosen. The vibrofore allows to perform HCF test in a short lapse of time of about 3 h thanks to high working frequencies, in the present research at 180 Hz. Tests have been performed at the three temperature levels investigated in the static tests, except for RT. This is because fati-gue damage occurs only at high temperature and because of the fragility of the alloy in this testing condition. For each specimen at least 30 min of hold time at the testing temperature before start-ing the test has been planned in order to avoid temperature gradi-ents. Experiments have been performed under sinusoidal pulsating tension loading conditions, adopting a stress ratio $R = 0.1$ in order to prevent crack closure during the propagation phase and to avoid reciprocal hammering of the fracture surfaces. As prescribed by UNI 3964 Standard, to complete the Staircase procedure, at least 15 specimens have been tested at each temperature level in order to estimate the 10%, 50%, and 90% reliability endurance limits. Then, the SN curves of the material at 50% of failure probability have been obtained through the application of the Maximum Like-lihood Method (MLM), as reported in [17,18]. The methodology allows to find the best fitting parameters for a given model and dis-tribution, accounting for both failures and run-out data and consid-ering a non-constant standard deviation too. A log-normal model was chosen to plot SN curves on a semi-logarithmic plane and the following distribution parameters (mean value and standard deviation) were used:

$$\begin{cases} \mu = \log N = C_0 + C_1\sigma + \frac{C_1}{\sigma} \\ S = \exp(D_0 + D_1\sigma) \end{cases} \quad (1)$$

where σ is the stress level, C_i and D_i are the coefficients to be calculated by maximizing the likelihood between the model and the experimental data through an algorithm based on the simplex search method [19].

Due to the fact that HCF tests have been performed at $R = 0.1$ conditions, a fatigue limit $\sigma_{D0.1}$ has been estimated. In order to evaluate the standard fatigue limit σ_{D-1} under symmetrical alternated load ($R = -1$), the adoption of the Haigh diagram has been needed to convert the fatigue limit values. For this purpose engineers, even for ductile steels or cast irons, commonly use the modified Goodman's model:

$$\frac{\sigma_a}{\sigma_{D-1}} + \frac{\sigma_m}{UTS} = 1 \quad (2)$$

To convert the $\sigma_{D0.1}$ in the σ_{D-1}, in the present work also the Gerber's model has been used because it is more conservative:

$$\frac{\sigma_a}{\sigma_{D-1}} + \left(\frac{\sigma_m}{UTS}\right)^2 = 1 \quad (3)$$

3. Tensile test results and discussion

The static tensile properties of the ductile cast iron investigated have been estimated as the mean values of at least 3 meaningful specimens for each testing condition. Table 2 summarizes the resulting numerical values.

In addition, Fig. 3 shows the stress–strain engineering curves corresponding to the investigated temperature levels.

As temperature increases, yield stress and tensile strength decrease with total elongation increasing. Work hardening occurs at room temperature resulting in a loss of ductility, which is confirmed also by the typology of failures, sometimes characterized by the detaching of small portions of material from the fracture surfaces. At 500 °C and 800 °C both the yield stress and ultimate tensile strength show a relevant decrease and elongation at break increases.

According with [2,5,6,20,21], these results suggest that higher levels of Si and Mo increase resistance of ductile iron at high temperatures by solid solution strengthening of Si and by precipitation strengthening of Mo carbides, respectively.

4. Thermal expansion coefficient estimation results and discussion

Fig. 4 shows the results obtained during the thermal expansion coefficient estimation, while Table 3 summarizes the resulting numerical values. In order to achieve a better approximation of the experimental data, three different regressions have been used for three different temperature ranges and, consequently, three values of the thermal expansion coefficient have been calculated.

5. HCF test results and discussion

The HCF results on the investigated ductile cast iron have been estimated by means of of at least 15 specimens and the HCF Stair-case method [16].

The run-out specimens of each Staircase specimen have been tested again at higher stress levels in order to increase the number of points defining the SN curves. Three equally spaced maximum stress levels have been defined between the estimated maximum stress fatigue limit and the UTS.

According to UNI 3964 Standard [16], i n Table 4 the computed fatigue limits in terms of maximum stress and corresponding standard deviation in $R = 0.1$ testing condition, stress amplitude $\sigma_{D0.1}$ and corresponding standard deviation under $R = 0.1$ testing condition and stress amplitude σ_{D-1} under $R = -1$ testing condition, estimated through the Gerber's model (3), are shown at different temperature levels.

For what concerns the scattering of HCF results, According to [10] the scattering of HCF limit results is very high for a cast iron.

Observing Table 4, it results that at 500 °C the fatigue limit in symmetrical loading condition at 50% of failures probability ranges about 65% of the fatigue limit at 160 °C, confirming the good properties of the material at high temperature.

The SN curves estimation has also allowed determining the constitutive parameters of the Basquin's stress-life relation [22] which links the elastic stress amplitude with the number of cycles to failure is:

Table 2
Tensile test results.

Temperature (°C)	Young modulus (GPa)	Yield stress (MPa)	UTS (MPa)	Elongation at break (%)
Room	178 ± 2.4	549 ± 25.9	608 ± 29.9	3.0 ± 0.9
160	173 ± 2.3	533 ± 17.8	594 ± 31.2	5.5 ± 1.2
500	141 ± 2.7	245 ± 16.9	352 ± 18.5	15.3 ± 1.9
800	116 ± 2.2	153 ± 21.3	154 ± 11.7	27.2 ± 2.0

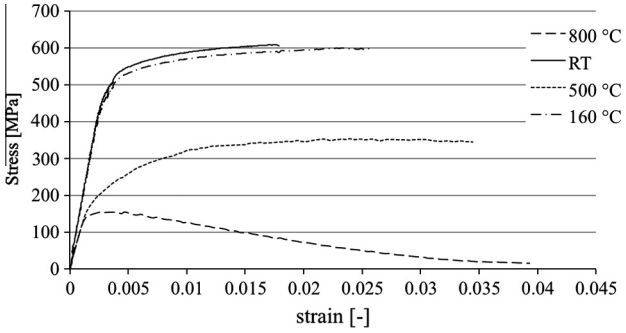

Fig. 3. Engineering tensile curves of the ductile cast iron.

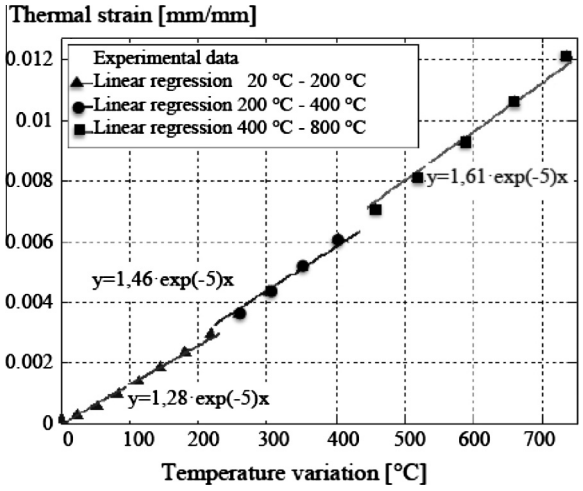

Fig. 4. Thermal expansion coefficient estimation.

Table 3
Thermal expansion coefficient values.

Temperature range (°C)	Thermal expansion coefficient (1/°C)
20–200	1.28×10^{-5}
200–400	1.46×10^{-5}
400–800	1.61×10^{-5}

$$\sigma_a = \sigma'_f (2N_f)^b \tag{4}$$

The material parameters σ'_f and b can be obtained by means of the high cycle fatigue data fitting procedure. As high cycle fatigue tests have been carried out under $R = 0.1$ loading conditions, the values of σ'_f and b have been calculated referring to $R = -1$ conditions. For this purpose the approximate construction of the SN curve [23] (Fig. 5) has been used, where the target endurance corresponding to the fatigue limit σ_{D-1} in $R = -1$ conditions has been fixed to 2×10^6 cycles.

The Basquin's curve parameter in $R = -1$ conditions can be then estimated by substituting the values of the UTS and fatigue limit σ_{D-1} obtained by means of the Staircase procedure, defining univocally the two fundamental points (0.9·UTS, 10^3) and (σ_{D-1}, 2×10^6) at each temperature level. The obtained results, imposing a confidence level of 95%, are reported in Table 5.

6. LCF test results and discussion

The LCF results of the ductile cast iron investigated have been estimated as the mean values of at least 3 meaningful specimens for each testing condition. The results are illustrated in terms of hysteresis loops shape and number of cycles to fracture, providing also metallographic observations to understand the material response.

At least 100 points for each cycle have been acquired during the low cycle fatigue tests in order to obtain the hysteresis cycle in the stress–strain plane. All the cycles have been acquired for elevated strain range tests, whose duration is shorter, while for the other conditions the first 100 cycles and then 1 cycle every 100 have been acquired.

Tests have been carried out until the failure of the specimen or until the load decreased by 50%. For each strain amplitude, the same temperature levels of the tensile tests have been investigated. The total strain ranges investigated, the temperature levels and the number of specimens are listed in Table 6; 160 °C represents the lowest working temperature of the exhaust manifold. According to [7] the material rapidly strain hardens, and later on during the test a slight softening takes place.

The stabilized hysteresis loops of the cast iron with 0.3% total strain amplitude at the different temperature levels (RT, 160 °C, 500 ° C, 800 ° C) are shown in Fig. 6, while the numbers of cycles corresponding to three meaningful specimens tested under each condition are reported in Table 7.

The last temperature level, equal to 800 °C, corresponds to the maximum working temperature of the actual component and it is reached only for few times during the component working period.

In Fig. 7 the values of the maximum and minimum peak stress for each cycle, acquired until the stabilization, are reported in order to appreciate the cyclic hardening or softening behavior of the material during the transient regime for RT LCF tests.

The stabilized hysteresis loops of the cast iron with 0.4% total strain amplitude at the different temperature levels (RT, 160 °C, 500 ° C, 800 ° C) are shown in Fig. 8; the numbers of cycles corre-sponding to three meaningful specimens tested under each condi-tion are reported in Table 8.

The values of the maximum and minimum peak stress for each cycle are reported in Fig. 9 for 160 °C LCF tests.

The stabilized hysteresis loops of the cast iron with 0.5% total strain amplitude at the different temperature levels (RT, 160 °C, 500 °C, 800 °C) are shown in Fig. 10; the numbers of cycles corresponding to three meaningful specimens tested under each condition are reported in Table 9.

The values of the maximum and minimum peak stress for each cycle are reported in Figs. 11 and 12 for 500 °C and 800 °C LCF tests respectively.

Table 4
HCF staircase results at 160 °C, 500 °C, and 800 °C.

% Failures	Fatigue limit	160 °C (MPa)	500 °C (MPa)	800 °C (MPa)
50	σ_{max}	185	116	74
	Standard deviation *s*	5	7	7
90	σ_{max}	178	107	65
10	σ_{max}	192	125	83
50	$\sigma_{D0.1}$	83	52	33
50	Standard deviation *s*	2	3	3
90	$\sigma_{D0.1}$	80	48	29
10	$\sigma_{D0.1}$	86	56	37
	Fatigue limit according to Gerber's model			
50	σ_{D-1}	86	53	34
90	σ_{D-1}	82	49	30
10	σ_{D-1}	89	57	38
	Fatigue limit according to modified Goodman's model			
50	σ_{D-1}	123	78	55
90	σ_{D-1}	117	71	47
10	σ_{D-1}	128	85	65

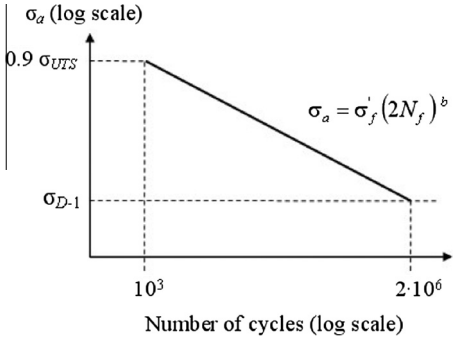

Fig. 5. Approximation of the SN curve.

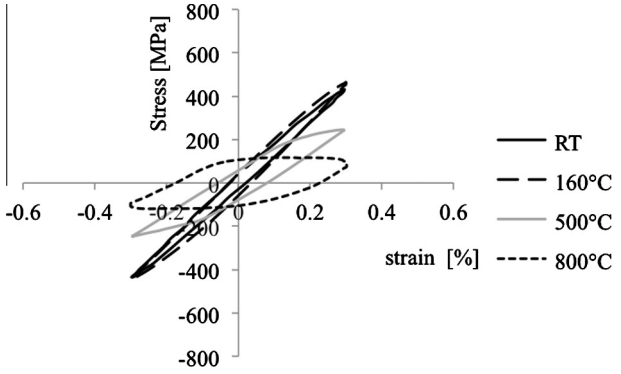

Fig. 6. Stabilized hysteresis loops, 0.3% of total strain amplitude at different temperatures.

Table 5
Estimated values of the Basquin's curve parameters in $R = -1$ conditions.

Temperature (°C)	σ_{D-1} (MPa)	*b* (–)
160	2857	−0.2205
500	1596	−0.2127
800	585	−0.1892

Table 6
LCF experimental test plan.

Total strain amplitude (%)	0.3, 0.4, 0.5
Temperature (°C)	RT, 160, 500, 800
Specimens tested	3

Table 7
Number of cycles to failure at 0.3% of total strain amplitude.

Specimen number	RT	160 °C	500 °C	800 °C
Sp 1	16	1351	3304	106
Sp 2	21	1280	3028	96
Sp 3	15	1640	3489	85
Mean	17.3	1423.7	3273.7	95.7
Standard deviation (%)	18.5	13.4	7.1	11.0

The material under investigation behaves as a fragile material at RT for all the testing strain ranges. The cycles to failure are few and the hysteresis cycle is small, the material thus dissipating a small amount of energy until fracture. This behavior is due to the presence of pearlite in the ferritic matrix that, in addition to Si, increases the strength of the alloy but it reduces its ductility at room temperature. The plot of the cyclic peak stresses at RT with 0.3% and 0.5% total strain (Fig. 7) shows that no evident cyclic hardening or softening behavior can be detected and the material response does not show evident transient regime before fracture. At 0.5% total strain amplitude and RT the shape of the cycle reveals the presence of an elevated plastic strain, which makes difficult to control the cycle even if the plot of the peak stress of the cycles achieved during the test shows that the material hardens at the beginning and then slightly softens.

Heating the material at 160 °C, the material ductility increases (Fig. 9). The number of cycles to failure in this condition increases with respect to RT of almost two orders of magnitude for 0.3% total strain amplitude and one order of magnitude for 0.5% total strain amplitude, even if the peak stresses and the size of the hysteresis loops are similar to those at RT. On the other side the corresponding tensile curves at 160 °C and RT are comparable for total strain amplitudes up to 0.5%. The material generally shows a moderate cyclic hardening behavior [24] that extinguishes after the first 20 cycles for 0.3% total strain amplitude, and after the first 50 cycles for 0.4%. In all cases, during the stabilized regime, both the minimum and maximum peak stresses can be assumed almost constant.

Moving to 500 °C (Fig. 11) the ductility of the material is still initially increasing and the number of cycles to failure is the great-

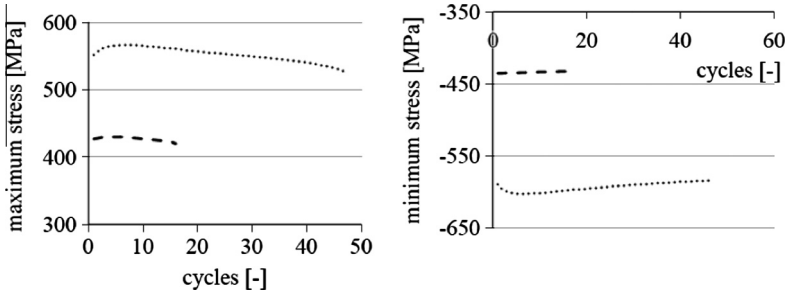

Fig. 7. Maximum (a) and minimum (b) peak loads, RT at different total strain amplitude: 0.3% dashed line, 0.5% dotted line.

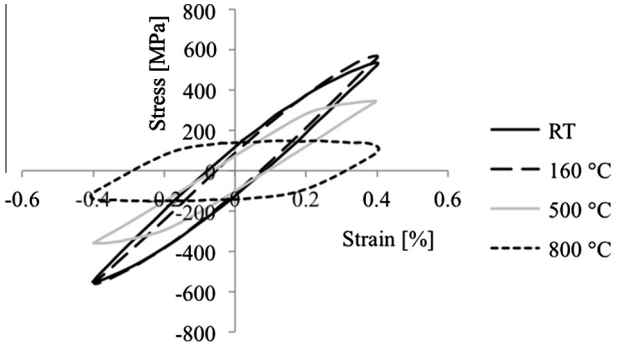

Fig. 8. Stabilized hysteresis loops, 0.4% of total strain amplitude at different temperatures.

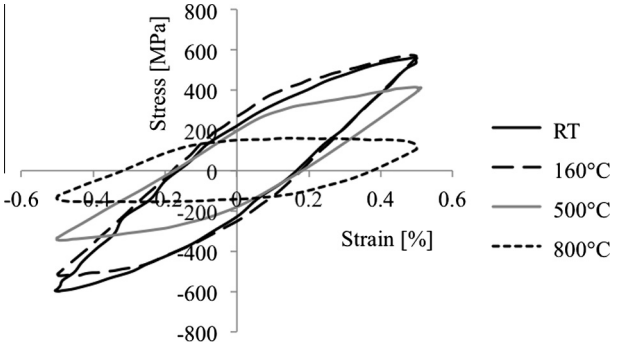

Fig. 10. Stabilized hysteresis loops, 0.5% of total strain amplitude at different temperatures.

Table 8
Number of cycles to failure at 0.4% of total strain amplitude.

Specimen number	RT	160 °C	500 °C	800 °C
Sp 1	44	781	1387	41
Sp 2	32	652	1208	47
Sp 3	40	712	1281	51
Mean	38.7	715.0	1292.0	46.3
Standard deviation (%)	15.8	9.0	7.0	10.9

Table 9
Number of cycles to failure at 0.5% of total strain amplitude.

Specimen number	RT	160 °C	500 °C	800 °C
Sp 1	46	452	818	34
Sp 2	51	324	809	28
Sp 3	41	401	741	33
Mean	46.0	392.3	789.3	31.7
Standard deviation (%)	10.9	16.4	5.3	10.2

est compared to all the other testing conditions. At this temperature, cycles show a significant plastic strain and a cyclic hardening behavior, as it can be appreciated in the plot of the hysteresis loops peak stresses in Figs. 6, 8 and 10 and in Fig. 13 which reports, as an example, the loading history for 0.4% total strain amplitude and 500 °C.

Moreover, at this temperature of 500 °C, the material shows a longer transient regime that extinguishes at about 250 cycles at 0.3% total strain amplitude and about 100 cycles at 0.4% and 0.5% total strain amplitude. The mechanical characteristics of the material decrease noticeably: cycles show a completely plastic behavior after yield. The cycle at 0.5% total strain amplitude shows a flat curve characterizing the loops in the plastic field. The peak stress history of Fig. 10 shows a tendency to soften cyclically without reaching a complete stabilization before failure.

Finally, at 800 °C, the mechanical characteristics of the material drop noticeably: cycles show a relevant plastic behavior after the yield (Figs. 6, 8 and 10). It is evident a tendency to soften cyclically without reaching a complete stabilization before failure. It is evident the change in the cyclic behavior between tests up to 500 °C, in which the cast iron shows a cyclic hardening response (Figs. 7, 9 and 11), and tests at 800 °C, where the material softens (Fig. 12).

It has to be noted that in all cases, the number of cycle to failure data scattering remains lower than 20% (Tables 7–9). Table 10

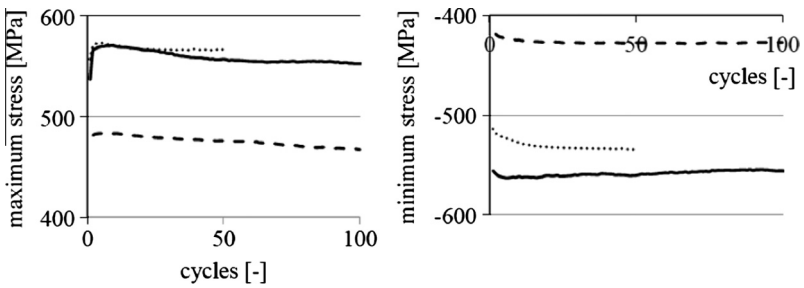

Fig. 9. Maximum (a) and minimum (b) peak loads, 160 °C at different total strain amplitude: 0.3% dashed line, 0.4% continuous line, 0.5% dotted line.

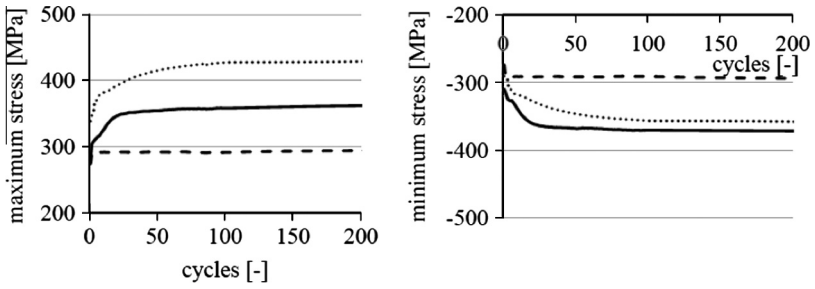

Fig. 11. Maximum (a) and minimum (b) peak loads, 500 °C at different total strain amplitude: 0.3% dashed line, 0.4% continuous line, 0.5% dotted line.

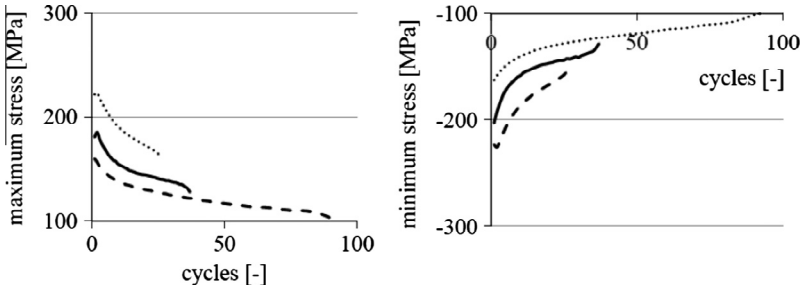

Fig. 12. Maximum (a) and minimum (b) peak loads, 800 °C at different total strain amplitude: 0.3% dashed line, 0.4% continuous line, 0.5% dotted line.

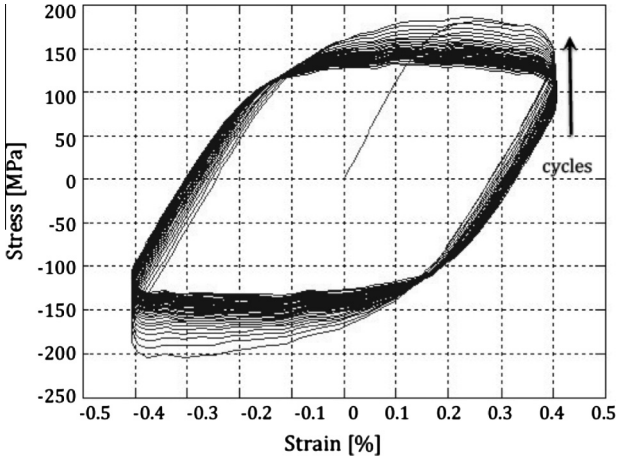

Fig. 13. Loading history example: 0.4% total strain amplitude, 500 °C.

summarizes the phenomenological features of the cast iron behavior, which arose from the LCF tests campaign. In particular, for each total strain amplitude and each temperature applied level, the cyclic response of the material and the number of cycles to reach the stabilized conditions is overviewed.

7. Microstructural observations

Some microstructural investigations have been performed. The selected images show density, size and distributions of the graphite nodules, and the composition of the matrix. In the following Figs. 14 and 15 the microstructure observed respectively at RT before fatigue tests and at 500 °C after LCF tests are shown.

Pearlite with about the same density and size is present in both sections, and also the graphite grains appear to be of the same density and size in the two images. This similarity can then justify the analogies in the trend of material response with temperature, with an increment of ductility when temperature increases. Pearlite grains are present; pearlite formation occurred at the ferrite grain boundaries, thus increasing the strength of the material but it decreases its ductility, in particular at RT.

Table 10
LCF tests summary.

Total strain amplitude	Temperature	Behavior	Number of cycles to stabilization
0.3%	RT	Not defined	–
	160 °C	Cyclic hardening	20
	500 °C	Cyclic hardening	250
	800 °C	Cyclic softening	–
0.4%	RT	Not defined	–
	160 °C	Cyclic hardening	50
	500 °C	Cyclic hardening	100
	800 °C	Cyclic softening	–
0.5%	RT	Not defined	–
	160 °C	Cyclic hardening	20
	500 °C	Cyclic hardening	100
	800 °C	Cyclic softening	–

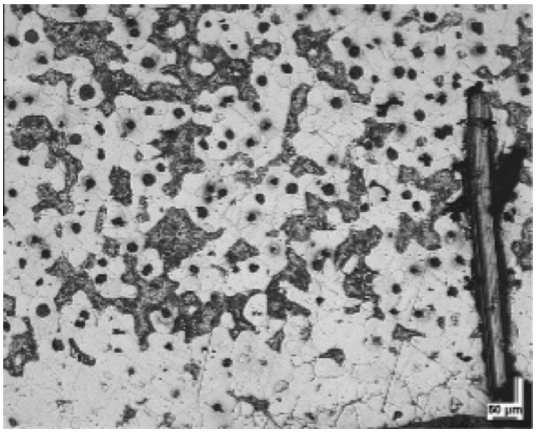

Fig. 14. Cast iron virgin material microstructure at 100× magnification.

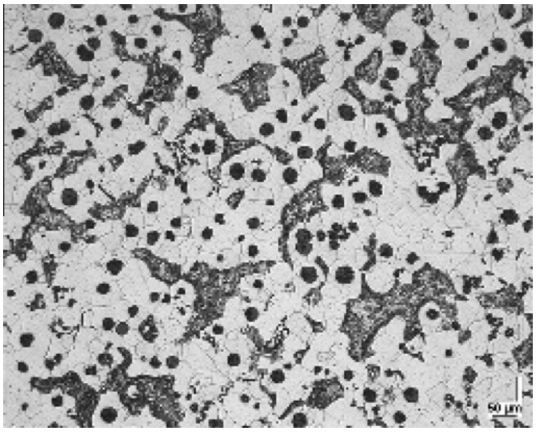

Fig. 15. Cast iron after 500 °C LCF fatigue testing at 100× magnification.

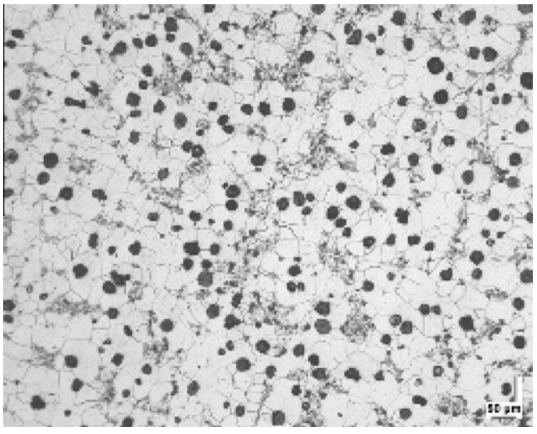

Fig. 16. Cast iron after 800 °C LCF fatigue testing at 100× magnification.

LCF tests show a change in the cyclic behavior between tests up to 500 °C, in which the cast iron shows a cyclic hardening response, and tests at 800 °C, where the material softens. Fig. 16 shows the microstructure at 800 °C.

In this case, while the grain size and density are almost equal to the previous temperature levels, no pearlite grains are detected, according with literature [21]. Such phase transformation behavior may justify the cyclic softening response of the material, as the lack of pearlite causes the lost of its major strengthening mechanism,

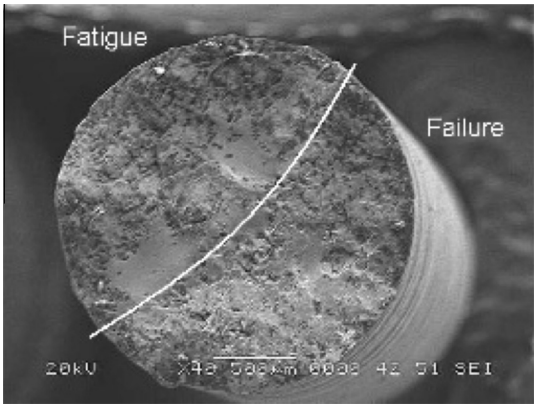

Fig. 17. Crack propagation and final failure zone, 160 °C, 40× magnification.

resulting in a lower strength and higher elongation than at the lower investigated temperature levels.

The peculiar features of the LCF failures have been investigated by several SEM observations. At 160 °C the fracture surface appears as in Fig. 17. Analyzing the crack propagation zone, it appears that the propagation has caused a mixed inter and trans-granular fracture where the first one is predominant near to the nucleation site, while the second one is more evident during propagation. The final resisting area is characterized by a trans-granular fracture. Moreover, in this zone it is possible to see also some sites of cleavage.

Moving to a broken low cycle fatigue specimen tested at 500 °C, an overall view of the fracture surface is shown in Fig. 18. In this

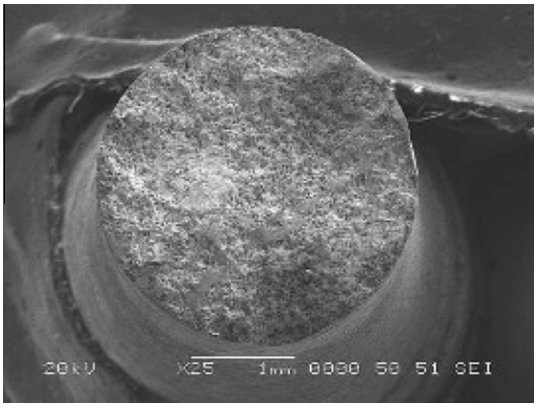

Fig. 18. Crack propagation and final failure zone, 500 °C, 40× magnification.

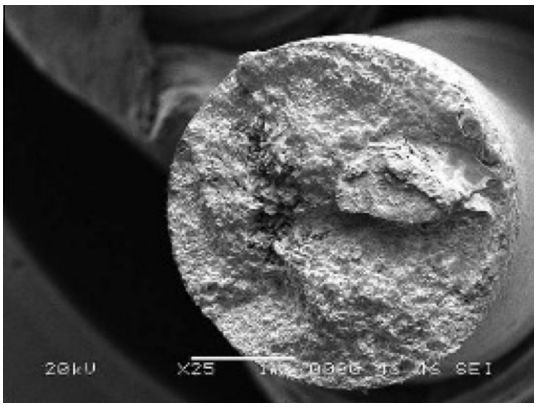

Fig. 19. Crack propagation and final failure zone, 800 °C, 40× magnification.

case it is more difficult to distinguish clearly the initial crack propagation zone from the final failure one, even if it can be asserted that the fracture is now completely trans-granular. The fatigue steps created during crack propagation are evident. In higher magnifications, graphite grains can be detected.

A fracture surface of a LCF specimen tested at 800 °C is shown in Fig. 19. Also in this case it is not clear where the crack probably nucleated and the fracture can be assumed as completely trans-granular. Graphite grains are quite evident, and the fracture surface appears to be in general ductile.

8. Conclusions

The temperature-dependent static and high cycle fatigue properties of a commercial ductile Si–Mo–Cr cast iron used in the manufacture of automotive exhaust manifold have been investigated. Based upon the results obtained, the following results may be pointed out.

Tensile tests show good mechanical properties of the alloy up to 500 °C. The high Si content causes a loss of ductility at low temperature levels, while on the other hand it assures good performances at high temperature. At 800 °C the material shows a drop in the mechanical properties mainly due to softening phenomena.

High cycle fatigue tests confirm the results of static tests. No fatigue test at room temperature has been performed due to the fragility of the alloy in this testing condition. Increasing the testing temperature the increase in ductility has allowed instead determining reliable results in terms of fatigue limits.

The research activity has allowed achieving some important results: the determination of the temperature-dependent elasto-plastic response, the microstructural evolution, and the failure features of this type of cast iron, about which the available literature is very poor.

On the other hand an optimized experimental plan that allows achieving good results with a small number of specimens and tests, with remarkable advantages in terms of time and costs, has been defined.

Acknowledgments

The Authors gratefully thank the kindness of prof. Narayanaswami Ranganathan, prof. Roger Serra and prof. René Leroy of Université François Rabelais in Tours, France.

References

[1] Chen PY, Lyons R, Rakoczy M, Otsuka K, Yamanaka H, Mimata T. Development of the 6.8l v10 heat resisting cast-steel exhaust manifold. SAE Technical Paper 962169; 1996.

[2] Park SH, Kim JM, Kim HJ, Ko SJ, Park HS, Lim JD. Development of a heat resistant cast iron alloy for engine exhaust manifolds. SAE Technical Paper 2005-01-1688; 2005.

[3] Fatahalla N, Abu El Ezz A, Semeida M. C, Si, and Ni as alloying elements to vary carbon equivalent of austenitic ductile cast iron: microstructure and mechanical properties. Mater Sci Eng A 2009;504:81–9.

[4] Brandes EA, Brook GB. Smithells metals reference book. Oxford: Butterworth Heinemann; 1992.

[5] Dodd J. Grey and nodular alloyed and high-strength Irons. Found Trade J 1979;147(8):963–1007.

[6] Li D, Perrin R, Burger G, McFarlan D, Black B, Logan R, et al. Solidification behavior, microstructure, mechanical properties, hot oxidation and thermal fatigue resistance of high silicon SiMo nodular cast irons. SAE Technical Paper 2004-01-0792; 2004.

[7] Meneghetti G, Ricotta M, Masaggia S, Atzori B. Comparison of the low-cycle and medium-cycle fatigue behaviour of ferritic, pearlitic, isothermed and austempered ductile irons. Fatigue Fract Eng Mater Struct 2013;36:913–29.

[8] Kumruoglu LC. Mechanical and microstructure properties of chilled cast iron camshaft: experimental and computer aided evaluation. Mater Des 2009;30:927–38.

[9] Hervas I, Ben M, Ben M, Ben Bettaieb M, Thuault A, Hug E. Graphite nodule morphology as an indicator of the local complex strain state in ductile cast iron. Mater Des 2013;52:524–32.

[10] Filipovic M, Kamberovic Z, Korac M, Gavrilovsk M. Microstructure and mechanical properties of Fe–Cr–C–Nb white cast irons. Mater Des 2013;47:41–8.

[11] Harkegard G, Svennson T, Zambrano HR. Round-robin prediction of the fatigue limit of a ring of spheroidal graphite cast iron. Fatigue Fract Eng Mater Struct 2012;36:382–91.

[12] Mellouli D, Haddar N, Köster A, Toure AML. Thermal fatigue of cast irons for automotive application. Mater Des 2013;43:272–82.

[13] Vadiraja A, Balachandrana G, Kamarajb M, Gopalakrishnac B, Prabhakara Raoc K. Studies on mechanical and wear properties of alloyed hypereutectic grey cast irons in the as-cast pearlitic and austempered conditions. Mater Des 2010;31(2):951–5.

[14] Vadiraja A, Balachandrana G, Kamarajb M. Effect of misch metal inoculation on microstructure, mechanical and wear properties of hypoeutectic grey cast irons. Mater Des 2009;30(10):4488–92.

[15] Vadiraja A, Balachandranb G, Kamarajc M, Kazuyad E. Mechanical and wear behavior of quenched and tempered alloyed hypereutectic grey cast iron. Mater Des 2011;32(4):2438–43.

[16] UNI 3964-1985. Mechanical testing of metallic materials – Fatigue testing at room temperature – General principles. UNI Standards; 1985.

[17] Goglio L, Rossetto M. Comparison of fatigue data using the maximum likelihood method. Eng Fract Mech 2004;71:725–36.

[18] Nelson W. Accelerated testing: statistical models, test plans, and data analyses. New York (USA): Wiley; 1990.

[19] Lagarias JC, Reeds JA, Wright MH, Wright PE. Convergence properties of the Nelder–Mead simplex method in low dimensions. SIAM J Opt 1998;9:112–47.

[20] Fairhurst W, Rohrig K. High silicon nodular irons. Found Trade J 1979;146:657–81.

[21] Kim YJ, Jang H, Oh YJ. High temperature low-cycle fatigue property of heat-resistant ductile-cast irons. Metall Mater Trans A 2009;40A:2087–97.

[22] Basquin OH. The exponential low of endurance tests. ASTM Proc 1910;10:625–30.

[23] Bannantine JA, Comer JJ, Handrock JL. Fundamentals of metal fatigue analysis. NJ (USA): Pretince Hall, Englewood Cliffs; 1990.

[24] Lemaitre J, Chaboche JL. Mechanics of solid materials. UK: Cambridge University Press; 2002.